

Mechanism of Beat Flow Formation for Three Side-by-side Prisms

Qinmin Zheng¹⁾ and *Md. Mahbub Alam²⁾

^{1), 2)} *Institute for Turbulence-Noise-Vibration Interaction and Control, Shenzhen Graduate School, Harbin Institute of Technology, Shenzhen, China*

²⁾ alamm28@yahoo.com; alam@hitsz.edu.cn

ABSTRACT

The flow over three side-by-side square prisms at $Re = 150$ is studied systematically at $L/W = 1.1 - 9.0$, where L is the prism center-to-center spacing and W is the prism width. Five distinct flow structures and their ranges are identified, viz., single bluff-body flow ($L/W < 1.4$), flip-flopping flow ($1.4 < L/W < 2.1$), symmetrically-biased beat flow ($2.1 < L/W < 2.6$), non-biased beat flow ($2.6 < L/W < 7.25$) and weak interaction flow ($7.25 < L/W < 9.0$). Physical aspects of each flow regime, such as vortex structures, gap flow behaviors, shedding frequencies and fluid forces are discussed in detail. A beat phenomenon or secondary frequency is observed in the symmetrically-biased and non-biased beat flows, influencing the lifts of the prisms to have a beat-like modulation. Difference in shedding frequencies resulted in the phase lag between the sheddings from two sides of a gap changing with the secondary frequency, which has a great impact on the lift force; the smaller the phase lag, the larger the lift amplitude. The modulation of lift amplitude thus stems from the phase lag change.

1. INTRODUCTION

Slender engineering structures are frequently arranged in groups, for example, high-rise buildings, chimney stacks, turning vanes in ducts, bridge piers, etc. Naturally, physics of flow around closely spaced structures is much more complicated than that around a single isolated structure, involving shear layer separation/reattachment, quasi-periodic vortices, mutual interactions, separation bubble, vortex impingement, structural vibration, noise, etc., which might aggravate the failure of the structures and the environmental pollutant transport in the vicinity of the slender structures in cluster. It is therefore significant in both fundamental research and practical applications to investigate the detailed physics of the flow around multiple closely spaced structures.

¹⁾ Graduate Student

²⁾ Professor

For two square prisms in side-by-side arrangement at $L/W = 1.02 - 6.00$, Alam, Zhou & Wang (2011) at $Re = 4.7 \times 10^4$ performed systematic measurements of the flow field, Strouhal number, time-averaged and fluctuating forces systematically. Four distinct flow regimes, namely (i) single-body regime ($1 < L/W < 1.3$), (ii) two-frequency regime ($1.3 < L/W < 2.2$), (iii) transition regime ($2.2 < L/W < 3.0$), and (iv) coupled vortex street regime ($L/W > 3.0$) were identified. Based on flow visualization experiments, qualitatively similar observations were further conducted at much smaller $Re = 300$ by Alam & Zhou (2013).

In the present study, we focus on detailed physics of the flow around three side-by-side square prisms. Simulations are performed at $Re = 150$ with $L/W = 1.1 - 9.0$, covering all possible flow regimes. Vorticity fields, shedding frequencies, time-averaged and fluctuating fluid force acting on the three prisms are analyzed to explicitly delineate the resultant flow structures.

2. COMPUTATIONAL DETAILS

2.1 Governing equations and boundary conditions

The dimensionless 2-D Navier-Stokes and continuity equations governing the flow of a Newtonian fluid can be written in vector form as

$$\left. \begin{aligned} \frac{\partial \mathbf{u}^*}{\partial t^*} + \mathbf{u}^* \cdot \nabla \mathbf{u}^* &= -\nabla p^* + \frac{1}{Re} \nabla^2 \mathbf{u}^* \\ \nabla \cdot \mathbf{u}^* &= 0 \end{aligned} \right\}, \quad (1)$$

where \mathbf{u}^* is the dimensionless flow velocity vector in the Cartesian coordinate system (x, y) with its two velocity components $u^* (= u/U_\infty)$ and $v^* (= v/U_\infty)$, $p^* (= p/\rho U_\infty^2)$ is the dimensionless static pressure, $t^* (= U_\infty t/W)$ is the dimensionless time, $Re (= \rho U_\infty W/\mu)$ is the Reynolds number, U_∞ is the freestream velocity, W is the prism width, ρ is the density of the fluid, and μ is the viscosity of fluid. The Re is kept constant at 150. The gravity force is excluded. The pressure-velocity coupling is handled with the pressure implicit with splitting of operators (PISO) method. Discretization of the convective terms is accomplished through a second-order accurate upwind differencing scheme, while the second-order implicit forward discretization is adopted for the time derivative terms. The length of the computational domain is taken to be $L_x = L_u + L_d$, where L_u is the upstream length and L_d is the downstream length from the coordinate origin at the center of the middle prism. The lateral computational boundaries each is $L/2$ away from the middle prism center. The boundary conditions are summarized as follows. At the inlet boundary, a uniform velocity profile ($u^* = 1, v^* = 0$) is imposed, while the stress vectors are set to zero at the outlet boundary ($\tau_{xx} = 2\mu(\partial u^*/\partial x^*) = 0, \tau_{yx} = \mu(\partial v^*/\partial x^* + \partial u^*/\partial y^*) = 0$). On the upper and lower lateral boundaries, the component of the velocity normal to and the component of the stress vector along the boundaries are prescribed a zero value ($v^* = 0, \tau_{xy} = \mu(\partial v^*/\partial x^* + \partial u^*/\partial y^*) = 0$). No-slip boundary condition ($u^* = v^* = 0$) is deployed on the surfaces of the square prisms. In the computational domain, the

initial flow velocities (at $t^* = 0$) are given as $u^* = 1$, $v^* = 0$, $p^* = 0$.

2.2 Validation of method and convergence of results

The first level of the grid spacing near the prism wall is set to be $0.0033W$ for an adequate resolution of the boundary layer, and increased with an expansion rate of 1.029 in the normal direction, while the size of cells along the perimeter of each prism is identical, $\approx 0.011W$. Table 1 compares the shedding frequency (St), fluctuating and time-averaged fluid forces (C'_L , C'_D and $\overline{C_D}$) obtained from the present cases with those from the literature for a single isolated square prism at $Re = 150$. The other parameters for the computations are $\Delta t^* = 0.0097$, $L_u/W = 13.5$, $L_d/W = 29.5$ and blockage ratio (BR) = $W/L_t = 5.26\%$. Here, the drag (C_D) and lift (C_L) coefficients and the Strouhal number (St) are calculated in the usual manner:

$$C_D = \frac{F_x}{\rho U_\infty^2 W / 2}, \quad C_L = \frac{F_y}{\rho U_\infty^2 W / 2}, \quad St = \frac{f_p W}{U_\infty} \quad (2)$$

where F_x and F_y are the drag and lift forces, respectively, comprising both pressure and friction forces on a unit length of the prism. f_p is the vortex shedding frequency, obtained by performing the fast Fourier transition (FFT) analysis of the lift coefficient signal. Overall, the integral parameters (St , C'_L , C'_D and $\overline{C_D}$) display a good agreement with those in the literature. The simulation for three side-by-side square prisms is thus given a similar mesh density and computational domain, i.e. $\Delta t^* = 0.0097$, $L_u/3W = 13.5$, $L_d/3W = 29.5$ and $BR = 3W/L_t = 5.26\%$.

Table 1. Comparison of the present results with those from the literature. $Re = 150$.

Sources	St	C'_L	C'_D	$\overline{C_D}$
Present case	0.1579	0.2770	0.0167	1.4827
Kumar, Sharma & Agrawal (2008)	0.1579	—	—	1.5296
Sharma & Eswaran (2004)	0.1588	—	—	1.4667
Saha, Biswas & Muralidhar (2003)	—	0.2740	0.0170	—
Sohankar, Norberg & Davidson (1999)	0.1650	0.2300	—	1.4400

3. FLOW STRUCTURES

Based on vortex structures, gap flow behaviors, fluid forces and shedding frequencies, five distinct flow regimes have been identified (figure 1). (i) Single-

bluff-body flow (regime *A*) identified at $L/W < 1.4$ is characterized by vortex shedding only from the freestream sides of the outer prisms, forming a single Karman vortex street. The flows through the gaps are insignificant or weak, failing to split the wake. Depending on the nature of the gap flows and their influence on the forces and wake, regime *A* is further subdivided into two sub-regimes: the perfectly single bluff-body regime ($L/W \leq 1.1$, insignificant flow through the gaps. figure 1a₁) and the single bluff-body-like regime ($1.1 < L/W < 1.4$, weak flow through the gaps. figure 1a₂). The weak gap flows interacting with the freestream-side shear layers postpone the vortex formation length and boost the shedding frequency and the convection velocity of vortices. The shedding frequency (St) thus being small ($St = 0.0470$ at $L/W = 1.1$), increases with an increase of L/W . (ii) Flip-flopping flow (regime *B*) appears at $1.4 < L/W < 2.1$ where the gap flows with appreciable vortices gain sufficient strength to split the wake into three, but the three wakes transmute into one shortly, with the vortices from the gap flows decaying, merging and pairing with the freestream side vortices. The two gap flows flip-flop in a chaotic manner, both to be biased upward, downward, outward, and straight (figure 1b₁ - b₄). The St compared to that at the single bluff-body flow jumps to 0.1440 (0.1379 - 0.1501, broad banded) for both outer prisms and 0.1690 (0.1630 - 0.1750, broad banded) for the middle prism. The flip-flopping of the wakes results in the broad banded St . The middle prism St is higher than the outer prisms', indicating that the middle prism undergoes the narrow wake most of the time where the two shear layers of the middle prism are squeezed inward (figure 1b₁ and b₂). (iii) Symmetrically-biased beat flow (regime *C*, $2.1 < L/W < 2.6$) features the two gap flows deflecting outward symmetrically. The two vortices from a gap interact with each other and also with the vortex from the respective freestream side vortex. The interaction results in occurrences of vortex integration and coupling between the gap flow and freestream side vortices. Note that, the two shear layers of the middle prism spawn vortices almost symmetrically, not alternately, in the upper and lower wakes. A substantial wide wake thus accompanies the middle prism, and a narrow wake complements each outer prism. The vortex sheddings from the outer prisms occurring at an identical frequency ($St = 0.1812$ at $L/W = 2.5$) are interlocked antiphase, with the shedding from the middle prism happening at a smaller frequency ($St = 0.1452$ at $L/W = 2.5$) (figure 1c₁ - c₂). (iv) Non-biased beat flow (regime *D*) taking place at $2.6 < L/W < 7.25$ is exemplified by the fact that the gap flows are not biased anymore; the wake of each prism is similar to that of an isolated prism. The sheddings from the outer prisms are interlocked with a constant phase lag, occurring at a smaller frequency than that of the middle prism ($St = 0.1721$ and 0.1833 for the outer and middle prisms, at $L/W = 3.5$). The instantaneous phase relationship between the vortex sheddings from the middle and outer prisms thus changes periodically. An interaction between the vortices from the gaps occurs, resulting in an irregularity of vortex arrangement and a decay of vortices particularly behind the middle prism (figure 1d₁ - d₂). (v) At $7.25 < L/W < 9.0$, weak interaction flow (regime *E*, figure 1e₁ - e₂) materializes, and the interaction between the

The 2016 World Congress on
Advances in Civil, Environmental, and Materials Research (ACEM16)
Jeju Island, Korea, August 28-September 1, 2016

vortices from the gaps is insignificant, with a small difference in shedding frequency between the outer and middle prisms.

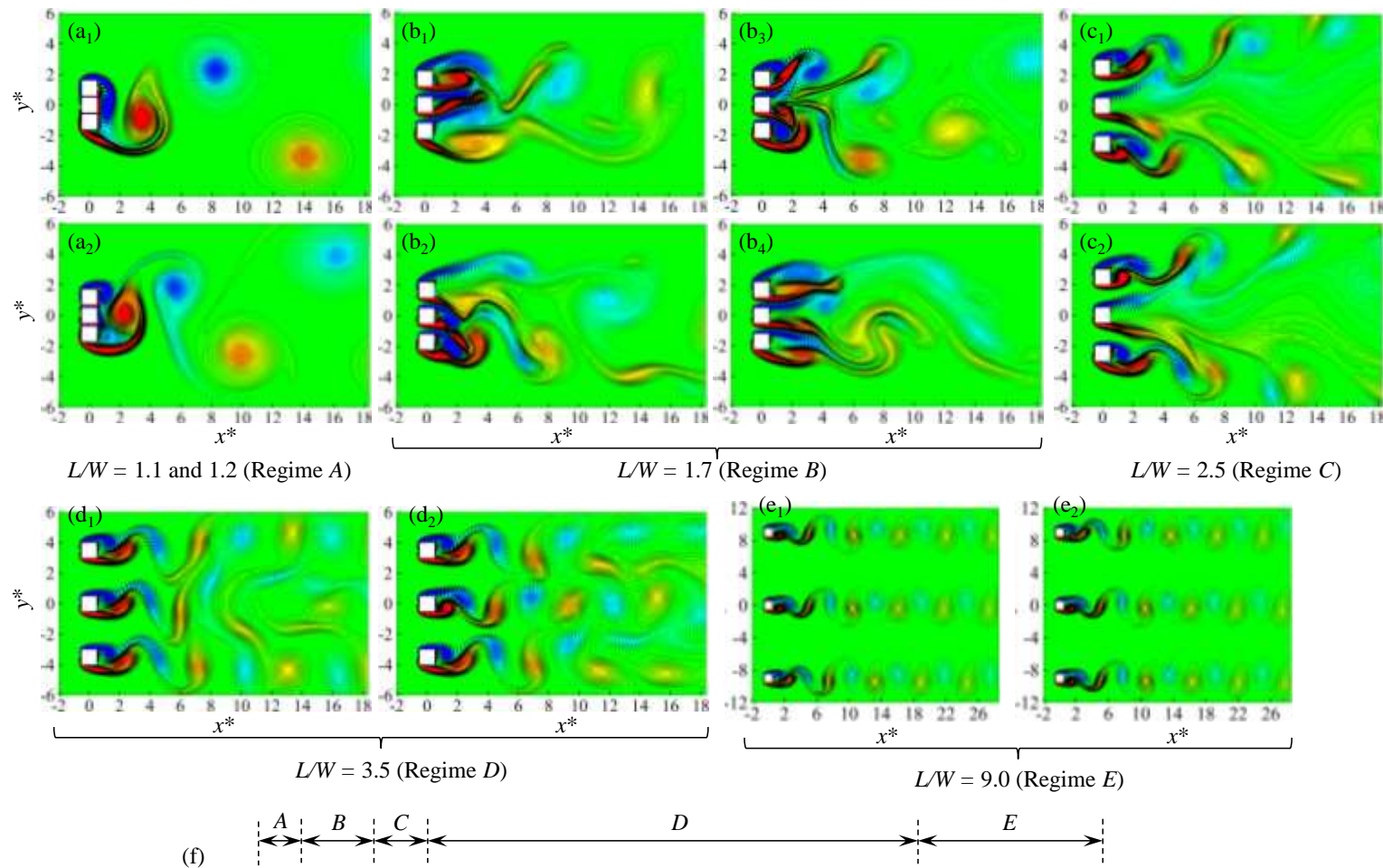


Fig. 1 Dependence of flow regimes on L/W and the typical flow structures: (a₁, a₂) regime A, single-bluff-body flow ($L/W < 1.4$); (b₁-b₄) regime B, flip-flopping flow ($1.4 < L/W < 2.1$); (c₁, c₂) regime C, symmetrically-biased beat flow ($2.1 < L/W < 2.6$); (d₁, d₂) regime D, non-biased beat flow ($2.6 < L/W < 7.25$); (e₁, e₂) regime E, weak interaction flow ($7.25 < L/W < 9.0$); (f) L/W range for each flow regime.

4. BEAT FLOW FORMATION MECHANISM

A beat phenomenon or secondary frequency is observed in the symmetrically-biased and non-biased beat flows, influencing the lifts of the prisms to have a beat-like modulation. For a detailed discussion, $L/W = 3.5$ is taken to be an exemplification (figure 2a). It is worth viewing the representative flow structures at maximum and minimum amplitudes (associated with the secondary frequency) of the lifts. The flow structures presented in figures 2(c) and (d) correspond to the maximum and minimum C_L -amplitudes ($t^* = 1836.3$ and 1877.4 , respectively) associated with the secondary frequency, as indicated by vertical lines in figure 2(a). Interestingly, the maximum C_L -amplitude (figure 2a) associated with the secondary frequency occurs when an inphase shedding occurs from the two sides of a gap (figure 2c). On the other hand, an antiphase shedding from the two sides of a gap (figure 2d) results in the minimum C_L -amplitude (figure 2a).

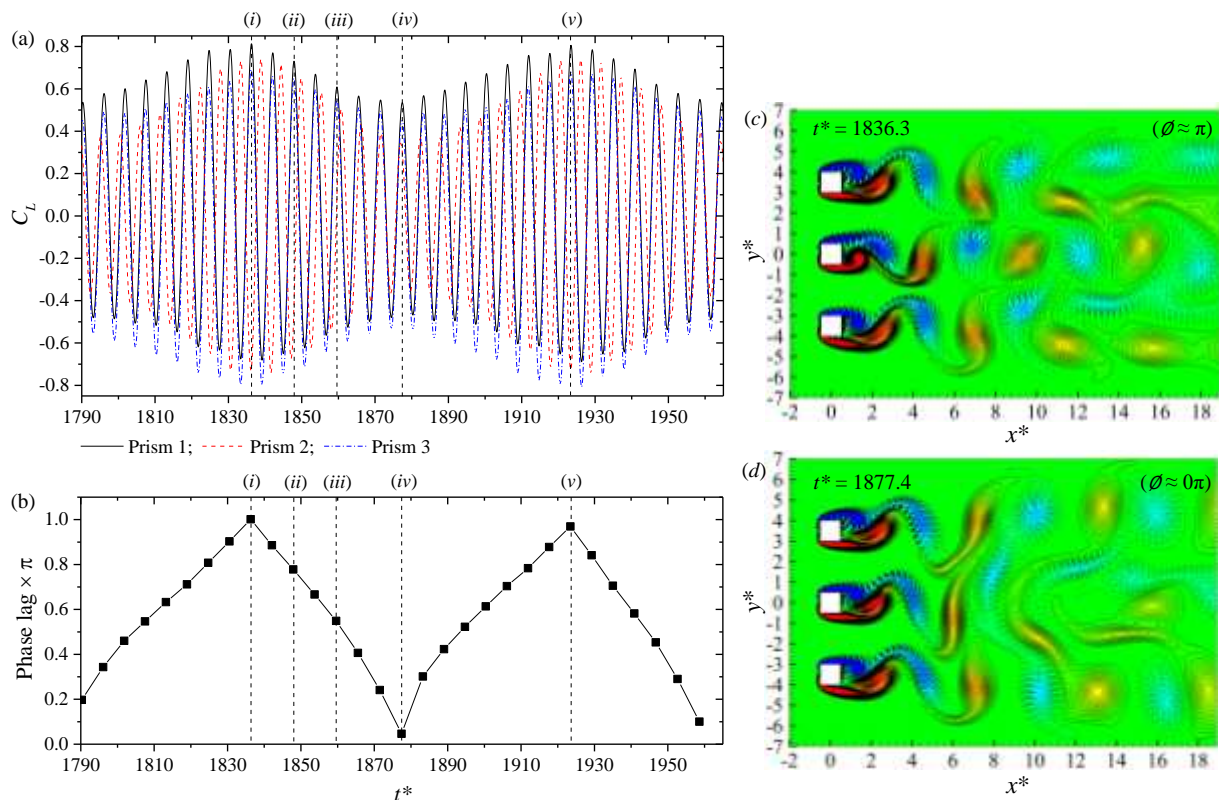


Fig. 2 (a) Time histories of lift coefficient acting on the three prisms. (b) Instantaneous phase lag between lift fluctuations of the upper and middle prisms. (c and d) Contours of instantaneous vorticity field showing vortex shedding from the prisms at $t^* = 1836.3$ and 1877.4 , respectively. $L/W = 3.5$. (i) $t^* = 1836.3$, (ii) $t^* = 1847.9$, (iii) $t^* = 1859.6$, and (iv) $t^* = 1877.4$.

Both gaps simultaneously may have inphase shedding (figure 2c) or antiphase

shedding (figure 2d), as the shedding phase lag between the outer prisms was a constant of $\approx 0^\circ$. C_L amplitudes of the three prisms thus reach their maxima or minima simultaneously. When the phase lag between the sheddings from the outer prisms is $\neq 0^\circ$, maximum or minimum lift amplitudes of the outer prisms do not occur simultaneously. So, the beat/secondary frequency results from a continuous change in the phase lag between the sheddings from the two sides of a gap, from inphase to antiphase, antiphase to inphase, and so on (figure 2b). Furthermore, the change in C_L amplitude of the middle prism also depends on the phase lag between sheddings from the outer prisms. Due to the different shedding frequencies from the two sides of a gap, the instantaneous phase lag changes in every primary period. It should not be confused that when the shedding frequencies are different, how can the phase lag be obtained? Here the phase lag means the phase of the longer period shedding (outer prism) with respect to that of the shorter period shedding (middle prism), i.e., considering the shorter period as a reference complete cycle period.

5. TIME-AVERAGED AND FLUCTUATING FLUID FORCES ON THE PRISMS

In this section, variation in fluid forces (time-averaged and fluctuating lift and drag coefficient, figure 3) acting on the three prisms with L/W will be discussed in detail and connect with the flow structures.

In regime A, vortex shedding only from the freestream sides of the outer prisms, and the gap flows between the prisms appear weak and dim at $L/W \leq 1.1$ (figure 1a₁), and become appreciably visible at $1.1 < L/W \leq 1.4$ (figure 1a₂). Consequently, the pressure on the inner side surfaces of the outer prisms is negligible, compared with that of the outer side surfaces. The difference of pressure gets smaller with an increase of L/W , responsible for the decreasing $\overline{C_{p1}}$ magnitude for the outer prisms ($\overline{C_{p1}} \approx 1.81$ at $L/W = 1.1$, and $\overline{C_{p1}} \approx 1.04$ at $L/W = 1.3$, figure 3a). Furthermore, the appreciable gap flows prolong the vortex formation and recover the convection velocity in the near wake. The negative pressure in the near wake thus gets weak, resulting in the decreasing $\overline{C_{p2}}$ magnitude, especially for the middle prism ($\overline{C_{p2}} \approx 4.32$ and 3.63 at $L/W = 1.1$ and 1.3 , respectively. figure 3b). Due to the effect of gap flows, the swerving of the shear layers weakens, the C_L' magnitude of the outer prisms thus decreases sharply, from 1.33 at $L/W = 1.1$ to 0.63 at $L/W = 1.3$. Furthermore, at $L/W = 1.2$, the swerving direction of both gap-flows with very small vortices was contingent on the shedding from the freestream sides, and the gap flows are less biased with relatively large inertia at $L/W = 1.3$. The C_L' magnitude of the middle prism thus increases and decreases ($C_L' \approx 0.544, 0.675$ and 0.620 for the middle prism at $L/W = 1.1, 1.2$ and 1.3 , respectively. figure 3c). The vortex formation occurs very close to the base of the middle prisms at $L/W \leq 1.1$ (figure 1a₁), and persists behind the outer prisms and moves downward due to the effect of the gap flows at $1.1 < L/W \leq 1.4$ (figure 1a₂). The C_D' magnitude of the middle prism thus decreases monotonously, while that of the outer prisms increases and decreases in the

$L/W \leq 1.1$ and $1.1 < L/W \leq 1.4$, respectively (figure 3d).

In regime *B*, a greater flow can pass through the gaps and split the wake into three immediately downstream of the prisms. The gap flows with relatively larger vortices flip-flop randomly at different fashions (figure 1b₁-b₄). A greater flow passing through the gaps diminishes the pressure difference between the outer and inner surface of the outer prisms, the $\overline{C_{D1}}$ magnitude for the outer prisms thus decreases with L/W (figure 3a). Besides, the two shear layers of the middle prism are largely squeezed inward, associated with a smaller formation length (L_f) and wake width (ω), while both formation length and wake width get large with an increase of L/W because of weakened squeezing effect. Here, L_f refers to the streamwise separation between the prism's center and the points of maximum fluctuating streamwise velocity in the wake, while ω refers to the transverse separation between the two maxima in fluctuating streamwise velocity contours (Alam, Zhou & Wang 2011). Consequently, the $\overline{C_{D1}}$ of middle prism decreases distinctly again, while that of the outer prisms also decreases, but slightly. Further, the C_{L1}^* magnitude of the middle prism is smaller than that of the outer prism, and both increases with L/W (figure 3c), implying that the gap flows swing with a more violent attitude. Furthermore, because the wake is chaotic, a long time statistical result gets a similar C_{D1}^* magnitude for the three prisms (≈ 0.32 , figure 3d).

In regime *C*, the gap flows are symmetrically biased outward; a reversed flow region thus form near the outer side surface of the outer prisms (figure 1c₁ and c₂), resulting in a slight increase of the $\overline{C_{D1}}$ magnitude for the outer prisms (figure 3a). As discussed above, a substantial wide wake accompanies the middle prism ($\omega \approx 2.45W$ at $L/W = 2.5$), and a narrow wake complements each outer prism. Consequently, the negative pressure in the near wake behind the middle prism is much smaller than that of the outer prisms and thus corresponds to the smaller $\overline{C_{D1}}$ magnitude (≈ 1.41). Further, the two shear layers of the middle prism spawn vortices almost symmetrically, not alternately, in the upper and lower wakes, resulting in the lower C_{L1}^* (≈ 0.030) and C_{D1}^* (≈ 0.094) magnitude (figure 3c and d).

In regime *D*, the gap flows are no longer biased where a single vortex street persists behind each prism (figure 1d₁ and d₂). The magnitude of $\overline{C_{D1}}$ for the outer prisms collapses from 0.59 ($L/W = 2.5$) to 0.18 ($L/W = 2.7$), and decreases gradually, converging towards zero (figure 2a). The magnitude of $\overline{C_{D1}}$ for each prism is close to each other, and decreases gradually with L/W (figure 3b), resulting from the increasing formation length ($L_f \approx 1.74W$ at $L/W = 2.7$ and $L_f \approx 2.14W$ at $L/W = 7.0$). Besides, C_{L1}^* of the middle prism thus has a distinct jump ($C_{L1}^* \approx 0.48$ at $L/W = 2.7$). The wake width of the middle prism is smaller than that of the outer prisms due to the squeezing effect from the inner shear layers of the outer prisms, while the difference of the wake width is diminishing with an increase in L/W ($\omega \approx 1.11W$ and $1.02W$ for the outer and middle prisms at $L/W = 2.7$, respectively, and $\omega \approx 1.03W$ and $1.0W$ at $L/W = 7.0$). The smaller wake width always corresponds to the smaller fluctuating fluid force (C_{L1}^* and C_{D1}^*), and thus the fluctuating fluid force (C_{L1}^* and C_{D1}^*) for both outer and middle prisms decreases

monotonously and converges toward that of an isolated prism (figure 3c and d).

In the regime *E*, the interaction between the wakes of adjacent prisms is weak. The shedding from each prism resembles that from an isolated prism, and the three vortex streets spaced sufficiently do not interact with one another (figure 1e₁ and e₂). The fluid forces ($\overline{C_L}$, C'_L , $\overline{C_D}$ and C'_D) for all three prisms are similar and close to those of an isolated prism.

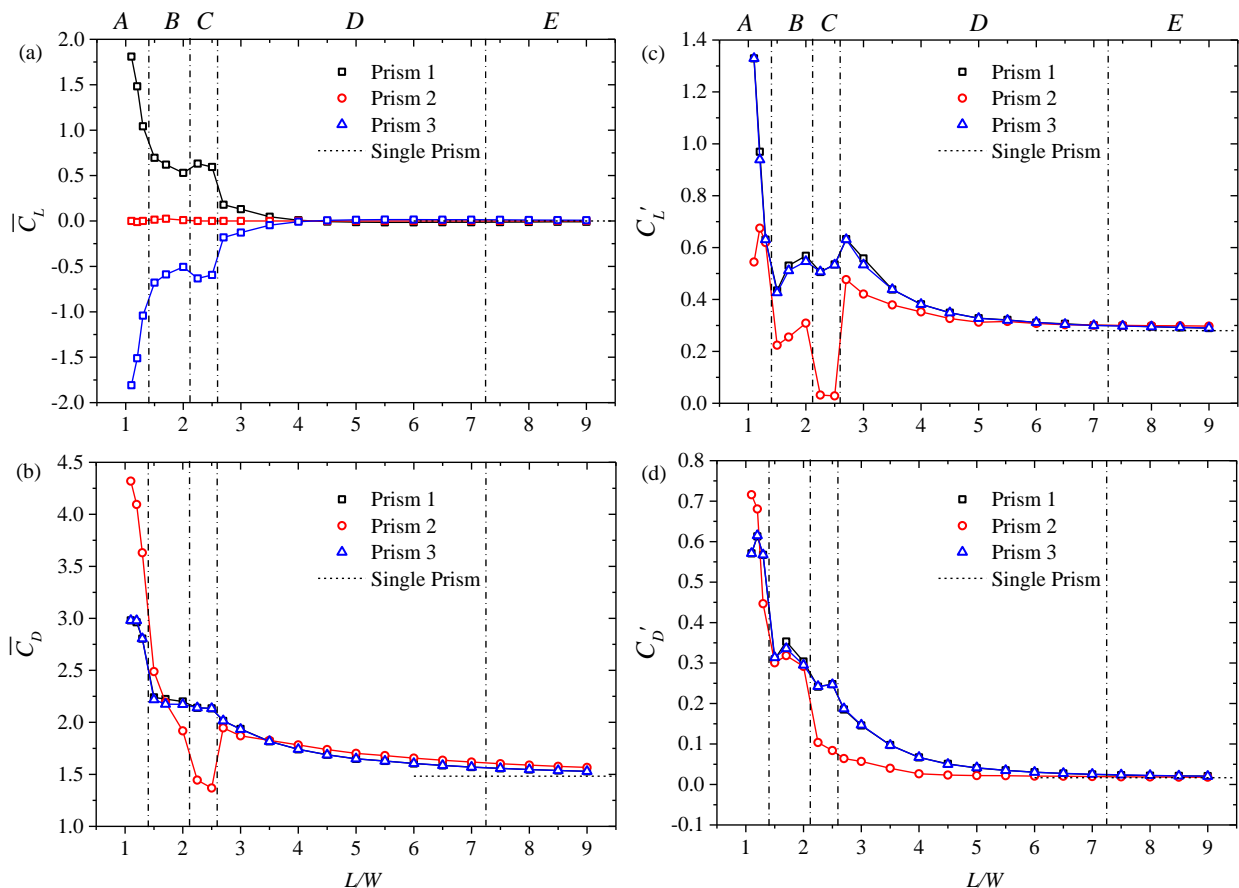


Fig. 3 Variation in (a) time-averaged lift ($\overline{C_L}$), (b) time-averaged drag ($\overline{C_D}$), (c) fluctuating lift (C'_L) and (d) fluctuating drag (C'_D) acting on the three prisms with L/W .

5. CONCLUSION

An investigation on the flow around three side-by-side square prisms can provide us a better understanding of complicated flow physics associated with multiple closely spaced structures where more than one gap flow is involved. A detailed study has been conducted on the wake of three side-by-side square prisms at $Re = 150$, with $L/W = 1.1 \sim 9.0$. Based on vortex structures, gap flow behaviors, shedding frequency and fluid forces, five distinct flow structures and their ranges are identified, viz., single bluff-body

flow ($L/W < 1.4$), flip-flopping flow ($1.4 < L/W < 2.1$), symmetrically-biased beat flow ($2.1 < L/W < 2.6$), non-biased beat flow ($2.6 < L/W < 7.25$) and weak interaction flow ($7.25 < L/W < 9.0$). A beat phenomenon or secondary frequency is observed in the symmetrically-biased and non-biased beat flows, influencing the lifts of the prisms to have a beat-like modulation. The secondary frequency results from the periodic change in phase lag between the sheddings from two sides of a gap. The phase lag has a great impact on the lift force; the smaller the phase lag, the larger the lift amplitude. The modulation of lift amplitude stems from the phase lag change. The dependence on L/W of fluid forces acting on the three prisms is discussed in detail, and connected with the flow structures.

ACKNOWLEDGMENTS

Alam wishes to acknowledge the support given to them from the Research Grant Council of Shenzhen Government through grant KQCX2014052114423867.

REFERENCE

- Alam, M. M. and Zhou, Y. (2013) "Intrinsic features of flow around two side-by-side square cylinders," *Phys. Fluids*. **25**.
- Alam, M. M., Zhou, Y. & WANG, X. W. (2011), "The wake of two side-by-side square cylinders," *J. Fluid Mech.* **669**, 432-471.
- Kumar, S. R., Sharma, A. and Agrawal, A. (2008), "Simulation of flow around a row of square cylinders," *J. Fluid Mech.* **606**, 369-397.
- Saha, A. K., Biswas, G. and Muralidhar, K. (2003), "Three-dimensional study of flow past a square cylinder at low Reynolds numbers," *Int. J. Heat Fluid Fl.* **24**, 54-66.
- Sharma, A. and Eswaran, V. (2004), "Heat and fluid flow across a square cylinder in the two-dimensional laminar flow regime," *Numer. Heat Transfer, Part A: Applications*. **45**, 247-269.
- Sohankar, A., Norberg, C. and Davidson, L. (1998), "Low - Reynolds - number flow around a square cylinder at incidence: study of blockage, onset of vortex shedding and outlet boundary condition," *Int. J. Numer. Meth. Fl.* **26**, 39-56.